Laboratory demonstration of geopotential measurement using transportable optical clocks

Dao-Xin Liu(刘道信)[1,2,3], Jian Cao(曹健)[1,2,†], Jin-Bo Yuan(袁金波)[1,2], Kai-Feng Cui(崔凯枫)[1,2], Yi Yuan(袁易)[1,2,3], Ping Zhang(张平)[1,2,3], Si-Jia Chao(晁思嘉)[1,2], Hua-Lin Shu(舒华林)[1,2], and Xue-Ren Huang(黄学人)[1,2,4,‡]

[1] *State Key Laboratory of Magnetic Resonance and Atomic and Molecular Physics, Innovation Academy for Precision Measurement Science and Technology, Chinese Academy of Sciences, Wuhan* 430071, *China*

[2] *Key Laboratory of Atomic Frequency Standards, Innovation Academy for Precision Measurement Science and Technology, Chinese Academy of Sciences, Wuhan* 430071, *China*

[3] *University of the Chinese Academy of Sciences, Beijing* 100049, *China*

[4] *Wuhan Institute of Quantum Technology, Wuhan* 430206, *China*

(Received 26 January 2022; revised manuscript received 29 March 2022; accepted manuscript online 1 April 2022)

We report an experimental demonstration of geopotential difference measurement using a pair of transportable $^{40}Ca^{+}$ optical clocks (TOC-729-1 and TOC-729-3) in the laboratory, each of them has an uncertainty of 1.3×10^{-17} and an instability of $4.8\times10^{-15}/\sqrt{\tau}$. Referenced to a stationary clock of TOC-729-1, the geopotential difference measurements are realized by moving TOC-729-3 to three different locations and the relevant altitude differences are measured with uncertainties at the level of 20 cm. After correcting the systematic shifts (including gravitational red shift), the two-clock frequency difference is measured to be $-0.7(2.2)\times10^{-17}$, considering both the statistic (1.0×10^{-17}) and the systematic (1.9×10^{-17}) uncertainties. The frequency difference between these two clocks is within their respective uncertainties, verifying the reliability of transportable $^{40}Ca^{+}$ optical clocks at the low level of 10^{-17}.

Keywords: geopotential difference measurement, transportable optical clock, repeatability evaluation of clocks

PACS: 06.30.Ft, 37.10.Ty, 37.10.Rs, 04.20.–q **DOI:** 10.1088/1674-1056/ac6337

1. Introduction

Recently, optical clocks have been improved greatly in uncertainty and instability with the technical development of cold atom and ultra-stable laser. The uncertainty or instability has reached the order of magnitude 10^{-18} or even better,[1–5] which is far exceeding the current second definition based on the Cs fountain clock. Therefore, high-precision optical clocks motivate the redefinition of the second in terms of an optical atomic transition.[6,7] In addition, optical clocks can also be used in relativistic geodesy,[8,9] precise measurement of physical constants,[10–13] and detection of dark matter.[14,15]

According to the Einstein's theory of general relativity (GR), a clock at a lower altitude runs slower than that at a higher altitude on the surface of the Earth due to the difference of the gravitational field, which is the so-called the gravitational red shift effect. By accurately measuring the frequency difference of the two optical clocks at separate locations through fiber or other links,[16–18] the related altitude difference can be acquired directly. This effect corresponds to a fractional frequency shift of about 1.1×10^{-18} per centimeter of change in altitude on the surface of the Earth, confirmed by several experiments by using optical clocks. In 2010, Chou *et al.* firstly demonstrated this effect using two $^{27}Al^{+}$ ion optical clocks with a resolution of 15 cm.[9] Thereafter, McGrew *et al.*[3] and Takano *et al.*[19] reported lattice clocks enabling geodesy at the centimeter level, respectively. Recently, Bothwell *et al.*[20] reported a millimeter-scale gravitational red shift measurement using the Sr lattice atomic clock, which is the highest resolution reported to date. These researches show us various opportunities of outdoor applications provided by optical clocks for establishing a global unified elevation network towards geophysics, satellites navigation, environmental monitoring, and resource exploration.[21]

However, optical clock is an ultra-precise and large equipment with considerable complexity, including atomic system and related laser-stabilization system, which limits the applicable scenario significantly. Thus, developing a transportable optical clock (TOC) with sufficient robustness and compactness is an effective solution for outdoor applications. At present, various institutions around the world are actively developing TOCs using different atomic references,[22–27] and some demonstrations on relativistic geodesy and test of the theory of GR have been reported now.[22,23]

The $^{40}Ca^{+}$ single-ion confined in an ion trap, due to its easy-to-acquired semiconductor lasers, is a promising option in the development of robust and compact TOCs. In addition, an excellent performance of systematic frequency uncertainty and instability makes it quite attractive and cost-

†Corresponding author. E-mail: caojian@apm.ac.cn
‡Corresponding author. E-mail: hxueren@apm.ac.cn

© 2023 Chinese Physical Society and IOP Publishing Ltd

effective. At present, several transportable single ion optical clocks (TOC-729-1, 2, 3) have been developed based on the $4s\ ^2S_{1/2} \leftrightarrow 3d\ ^2D_{5/2}$ electric quadrupole transition of $^{40}Ca^+$ in Wuhan. These three TOCs are based on the previous work[24] with improvements to the modular and integrated design of clocks, upgraded controlling system, suppressed systematic shifts and related high precision evaluation. For TOC-729-2, its outer size of the physical package is 1.2 m × 0.9 m × 0.3 m apart from the controlling electronics placed in 19-in. racks. It was moved 1200 km from Wuhan to Beijing by express delivery and then resumed to work quickly, and its systematic uncertainty was reevaluated as 1.1×10^{-17}, which remained almost the same as in Wuhan. This TOC shows a high uptime of 92% in 35 days of absolute frequency measurement and will be used to steer the local time scale.[28]

In this paper, a pair of TOCs is used to demonstrate the geopotential difference measurement in the laboratory. Referenced to the stationary TOC-729-1, the geopotential difference measurements are performed by moving TOC-729-3 to three different altitudes. The fractional frequency difference changes are measured at the level of 2.0×10^{-17}, corresponding to an altitude uncertainty at 20 cm level. Meanwhile, to analyze the reproducibility of these two TOCs, the frequency difference between them is evaluated to be $-0.7(2.2) \times 10^{-17}$, including both the statistic and systematic (gravitational red shift included) uncertainties at three different altitudes. This result is consistent well with the systematic uncertainties of the two clocks, demonstrating the reliability of TOCs for elevation measurements at the uncertainty level of 20 cm. This work is meaningful as a preliminary preparation for establishing a global unified elevation network and for the testing of fundamental physics laws.

2. Experimental details

The two transportable $^{40}Ca^+$ optical clocks (TOC-729-1 and TOC-729-3) used for geopotential difference measurements have a similar structure. The same vacuum chambers and linear Paul traps are employed. In addition, these two traps are worked at the magic radio-frequency (24.801 MHz) to eliminate the frequency shifts due to excess micromotion.[29] These two clocks share a common 729 nm cavity-stabilized diode laser system as the local oscillator,[30] and other related lasers (397 nm/854 nm/866 nm) are stabilized by a 3-in-1 cavity to suppress long-term frequency drifts.[24] A high-resolution timing controlling system based on the field-programmable gate arrays (FPGAs) is shared temporarily, which can achieve fast timing sequence with a resolution of nanosecond level. In the comparisons, the probe pulses of the clock laser for the two TOCs are precisely synchronized, which allows two clocks to sample the same laser noise. Therefore, the frequency difference between them benefits from a common-mode rejection of the laser noise.

In addition to the above commons, these two clocks have different ways of loading ions. TOC-729-1, similar to TOC-729-2, uses a calcium oven to load a single ion, but TOC-729-3 uses the laser-ablation method[31] alternatively. A pulsed laser at 1064 nm acts as an ablation source controlled by an acousto–optic modulator (AOM). This method can quickly and stably load a single ion without contaminating the trap electrodes by precisely controlling the power and pulse-time of the ablation laser.

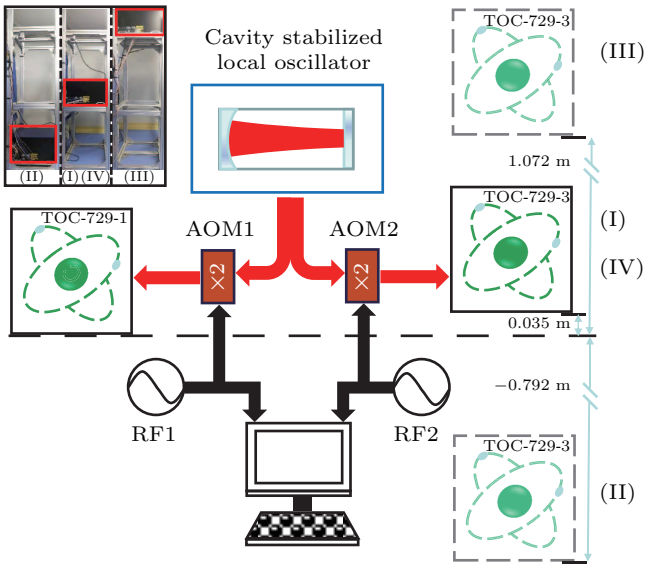


Fig. 1. Schematic diagram of the geopotential difference measurements. TOC-729-1 and TOC-729-3 share a cavity-stabilized clock laser at 729 nm, which is split and sent to each ion trapping module of the clock system. To ensure each optical clock has independent frequency control of clock laser beams, TOC-729-1 and TOC-729-3 have been equipped with separate AOMs. The 729 nm laser frequency is locked to the clock transition using a digital servo that provides a correction to the AOM driver for the corresponding clock. The geopotential difference measurements are performed at three different altitudes between two clocks of $-0.792(10)$ m, $0.035(10)$ m, and $1.072(10)$ m, respectively. Inset on the top left shows the actual physical system of TOC-729-3 when it was placed at three different altitudes.

The workflow of the clocks from the preparation to operation is kept the same to each other. After a single ion is loaded, various experimental parameters should be inspected and optimized. The compensation electrodes of the ion trap are optimized by using a parametric excitation method[32] to minimize the excess-micromotion. The Doppler-cooling parameters of the single ion are optimized to ensure the time dilation shift due to the secular motion remains stable. Two sensors (PT1000) are pasted on the vacuum chamber of the ion-trapping module to record the temperature during the comparison, and the data is employed to evaluate the black-body radiation (BBR) shift. A frequency-resolved optical pumping method[33] is employed for state preparation to double the transition probability and improve the clock instability by $\sqrt{2}$ times. For all measurements presented in this paper, a Rabi interrogation time of 60 ms is performed for clock operation,

corresponding to a Fourier limited linewidth of 13.3 Hz. The optical frequency is locked to the electrical quadrupole transition at 729 nm by feeding the frequency corrections back to the rf driver of AOM. This rf frequency is recorded to determine the difference between the two clocks. During the geopotential difference measurement, as shown in Fig. 1, TOC-729-1 is placed on the optical platform as a reference, and the ion-trapping module of TOC-729-3 is encapsulated in a box of 0.62 m × 0.50 m × 0.34 m for moving conveniently in the order of (I) → (II) → (III) → (IV).

3. Experimental results

3.1. Geopotential difference measurement

According to the GR, the gravitational red shift between the clocks ($\Delta\upsilon = \upsilon_2 - \upsilon_1$) located at positions 1 and 2 is given by their relative altitude difference (Δh) as $\Delta\upsilon/\upsilon_1 = (1+\alpha)g\Delta h/c^2$, where $\upsilon_{1(2)}$ is the clock transition frequency at location 1 (2), g is the gravitational acceleration, c is the speed of light, and α indicates a violation factor of the GR. The geopotential difference measurements are realized assuming $\alpha \approx 0$. As shown in Table 1, at three different altitudes, the frequency differences between TOC-729-1 and TOC-729-3 are measured as −46.5(5.2) mHz, −12.8(4.8) mHz, and 38.1(4.2) mHz, respectively.

Table 1. Results of the geopotential difference measurements at three different altitudes. Unit: mHz.

$\Delta H_{\text{clock 3–clock 1}}$ (m)	Clock 3–Clock 1		
	Statistical	Systematic	Total
−0.792(10)	−46.5(5.2)	−9.4(7.3)	−37.1(9.0)
0.035(10)	−12.8(4.8)	−10.4(7.8)	−2.4(9.2)
1.072(10)	38.1(4.2)	−7.4(8.7)	46.5(9.7)

After correcting the systemic shifts of −9.4(7.3) mHz, −10.4(7.8) mHz, and −7.4(8.7) mHz, the final frequency differences at three different altitudes are synthesized to be −37.1(9.0) mHz, −2.4(9.2) mHz, and 45.5(9.7) mHz, respectively. Detailed experimental data is shown in Fig. 2(a). The fractional frequency shifts are calculated as $-9.0(2.2)\times10^{-17}$, $-0.6(2.3)\times10^{-17}$, and $11.1(2.4)\times10^{-17}$. Based on $\Delta\upsilon/\upsilon_1 = g\Delta h/c^2$, where g is 9.793461(2) m/s^2 obtained from an atomic gravimeter,[34] the altitude differences are calculated as −0.83(20) m, −0.05(21) m, and 1.02(22) m, in agreement with the measurement of −0.792(10) m, 0.035(10) m, and 1.072(10) m using a meter ruler.

On the contrary, these measurements can be analyzed by using $\Delta\upsilon = k\Delta h$ to test the GR, where k is defined as $(1+\alpha)\upsilon_1 g/c^2$. As shown in Fig. 2(b), the slope k is 0.0444(12), and α is calculated as $-9(27)\times10^{-3}$. GR verification is an important step in the testing of the fundamental physical laws. However, the measurement precision of α is limited by the uncertainties of the clocks and the altitude difference between them. The Gravity Probe A mission[35] obtains $|\alpha| \approx 1.4\times10^{-4}$ by using a hydrogen maser in a spacecraft launched to $\Delta h = 10^4$ km, which is benefited a lot from the large scale of altitude difference. The accuracy of the optical clocks is 5 to 6 orders of magnitude better than that of hydrogen masers, so we can obtain more precise α with an appropriate altitude difference. For example, Takamoto *et al.*[23] operated a pair of transportable Sr lattice clocks with an altitude difference of $\Delta h \approx 450$ m at Tokyo Skytree to measure α as $(1.4\pm9.1)\times10^{-5}$. Its accuracy has already surpassed the result by using hydrogen masers.[35] By improving the uncertainty of our TOCs to 5×10^{-18} and increasing the altitude difference to about 5 km, the uncertainty of α will be measured as 8.9×10^{-6} to perform a more precise test of GR in the future.

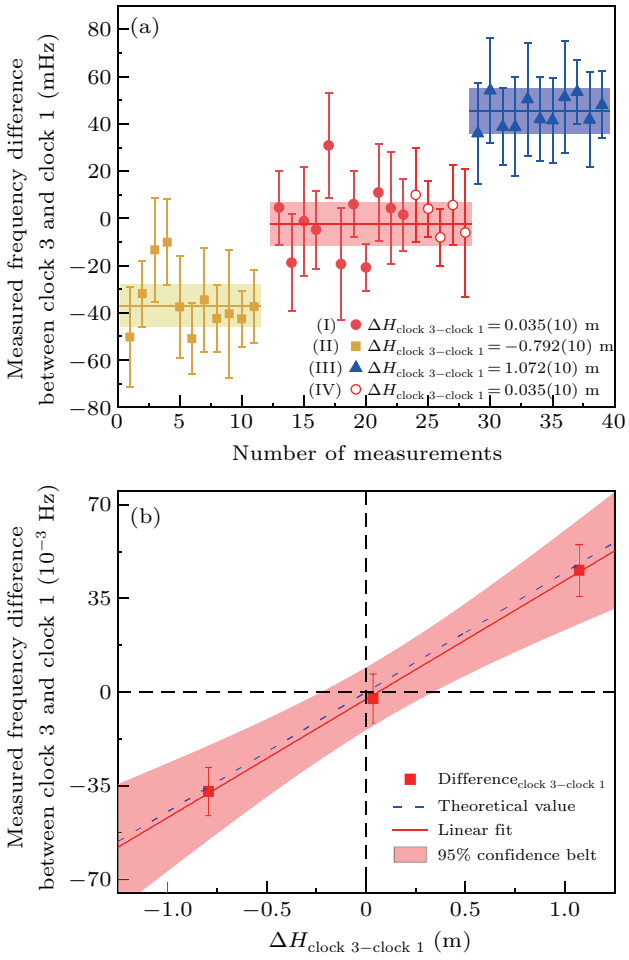


Fig. 2. Results of the geopotential difference measurements at three different altitudes. (a) The 38 points of measurement data. Each data point is corrected with the systematic shifts (gravitational red shift excluded). The solid line and shadowed area represent the weighted mean and the corresponding standard deviation. The red hollow circle data points are taken after moving TOC-729-3 to its initial position, to verify the repeatability of the clock. (b) The relationship between the frequency differences and the altitude differences. The red dots represent the measurement data, and the red solid line indicates the linear fit of them. The blue dashed line with the slope of 0.04479(3) is the theorized expectation according to the local gravitational acceleration. The shaded red area represents the 95% confidence intervals.

3.2. Repeatability evaluation of clocks

To evaluate the repeatability of these two clocks, two sets of measurements are performed at the same location ($\Delta H_{\text{clock 3–clock 1}} = 0.035(10)$ m) with an interval of a month. The results are consistent with the uncertainty as shown in Fig. 2(a). Due to TOC-729-3 moving within the range of 2 m altitude difference in the laboratory, the change of gravitational acceleration can be ignored, and the more accurate evaluation of gravitational red shift can be obtained from the geometrical measurement with a meter ruler. After correcting the gravitational red shifts at three different altitudes with this method, as shown in Fig. 3, a fractional instability of $4.8 \times 10^{-15}/\sqrt{\tau}$ is achieved for both TOCs, which is reasonable agreement with the QPN limit of $3.1 \times 10^{-15}/\sqrt{\tau}$. The frequency difference between the two TOCs is calculated as $-0.7(2.2) \times 10^{-17}$ with the statistic uncertainty of 1.0×10^{-17} and the systematic uncertainty of 1.9×10^{-17}. This systematic uncertainty is derived from the synthesis of the uncertainty of each clock at the level of 1.3×10^{-17}. The frequency difference is consistent well with the systematic uncertainties of two TOCs, which verifies the reliability of TOCs for geopotential difference measurements at the uncertainty level of 20 cm.

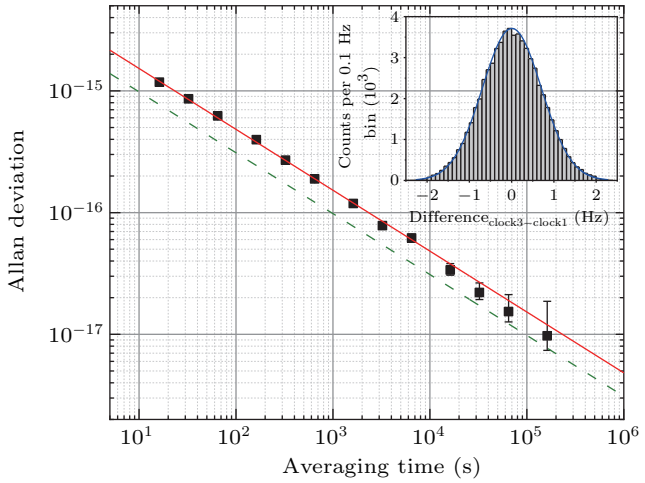


Fig. 3. The Allan deviation measured for each clock. The frequency difference between the two clocks is divided by $\sqrt{2}$ to reflect the instability of a single clock. The red solid line shows the $1/\sqrt{\tau}$ fit of the data yielding an instability of a single clock as $4.8 \times 10^{-15}/\sqrt{\tau}$. The green dash line stands for the theoretical predicted quantum projection noise (QPN) limit of $3.1 \times 10^{-15}/\sqrt{\tau}$, calculated under the condition of 16.2 s feedback time.[36] Inset: Statistical distribution of the frequency difference between the two clocks after correcting the systematic shifts.

The systematic frequency shift uncertainties of the optical clocks are the most important factor limiting the accuracy of the geopotential difference measurement, and its evaluation is also an important part of the repeatability evaluation of the optical clock. The details about the main sources of errors in the clock evaluation are described below.

For our $^{40}Ca^{+}$ optical clock, the systematic uncertainty is limited by the BBR related frequency shift, as shown in Table 2. To evaluate this item, the environment temperature seen by the ion needs to be measured with high precision. However, this is quite difficult due to the non-uniform temperature distribution caused by the heating effect of the rf driving. However, we have proposed an improved BBR temperature evaluation method[37] based on the analysis of the effective solid angle of each component of the ion trap system using the finite element method. By combining with the temperature of each component measured in a dummy trap system, the effective temperature felt by the ion can be calculated. The vacuum chamber temperature, monitored by calibrated PT1000 sensors, is 295.89(55) K for TOC-729-1 and 294.32(66) K for TOC-729-3. According to the temperature distribution model of ion trap established, the effective temperature felt by the ion is calculated respectively as 296.69(77) K and 294.83(84) K, corresponding to a BBR ac-Stark shift uncertainty of 3.8 mHz and 4.1 mHz.

Table 2. Systematic shifts and uncertainties for the evaluations of the two TOCs. All values shown here are in millihertz except for the last row.

Effect	Clock 1		Clock 3	
	Shift	Uncertainty	Shift	Uncertainty
Thermal motion 2nd-Doppler	−1.1	0.1	−1.0	0.1
Intrinsic micromotion	0	< 0.1	0	< 0.1
Excess micromotion	0	< 0.1	0	< 0.1
Blackbody radiation ac-Stark	363.1	3.8	354.0	4.1
Blackbody radiation 2nd-Zeeman	0	< 0.1	0	< 0.1
Bias magnetic 2nd-Zeeman	0.1	< 0.1	0	< 0.1
Bias magnetic linear-Zeeman	0	0.3	−0.8	1.1
Electric quadrupole	0	3.8	0	3.2
Servo	−0.2	0.6	0.2	0.6
729 nm laser ac-Stark	0.1	< 0.1	0.1	< 0.1
Other laser ac-Stark	0	< 0.1	0	< 0.1
Collision	0.6	0.5	0.6	0.5
First-order Doppler	0	< 0.1	0	< 0.1
AOM chirping	0	< 0.1	0	< 0.1
Line pulling	0	< 0.1	0	< 0.1
Total	362.6	5.4	353.1	5.4
Relative uncertainty (10^{-17})	88.2	1.3	85.9	1.3

The electric quadrupole frequency shift is caused by the interaction of the electric quadrupole moment of the $^2D_{5/2}$ level with the electric field gradient. In order to eliminate this kind of shift effectively, three pairs of Zeeman components labeled $m_j = \pm 1/2$, $m_j = \pm 3/2$, and $m_j = \pm 5/2$ are detected alternately.[38] The average value of the center frequencies of three pairs of lines is used as the output of the clock. The uncertainty of the electric quadrupole shift can be estimated by evaluating the difference of center frequencies among the three pairs of lines.[24] During all the geopotential difference measurements, the electric quadrupole shift uncertainty is measured to be 3.8 mHz and 3.2 mHz for TOC-729-1 and TOC-729-3, respectively.

The linear Zeeman shift can be canceled out effectively by probing on three pairs of symmetrical Zeeman components.

However, as these components can only be detected alternately, the drift of the magnetic field will produce a residual linear Zeeman shift of 16.8 Hz/nT by a worst-case scenario. Due to the proximity to the subway, the environmental magnetic field can fluctuate as much as 1000 nT. Although there are two layers of the magnetic shields, the residual magnetic field drift at the ion position calculated from the frequency records during the clock operation is at the level of 10^{-5} nT/s, which is a little higher than that of TOC-729-2 as it is far from the subway.[28] Considering the 2.7 s probing interval between each Zeeman component, the linear Zeeman shift uncertainty is estimated to be 0.3 mHz for TOC-729-1 and 1.1 mHz for TOC-729-3.

The servo error is also an important item in the systematic uncertainty of a single ion optical clock, which is caused by the long servo feedback time and the inevitable frequency drift of the clock laser referenced to an ultra-stable cavity. Two methods are employed to reduce the servo feedback period of the clock. The first is using state preparation to reduce the feedback time of clock servo, and the second is using a high-speed FPGAs controlling system to reduce the dead time in the sequence of laser pulses. As a result, the total feedback time is reduced from 32.2 s to 16.2 s dramatically with a constant 60 ms probe time. For the frequency drift of the clock laser, a linear drift compensation with refreshed data intermittently is superimposed to the AOM before the ultra-stable cavity, and the residual frequency drift of the probe laser can be controlled within ± 5 mHz/s. In addition, a second-order integral is added to the clock servo loop,[39] thereby reducing the servo error caused by the frequency drift of the ultra-stable cavity. With these efforts, the final servo error uncertainty is suppressed to 0.6 mHz for both clocks.

In addition to the main sources mentioned above, all other items are at the level of 1.0×10^{-17} or even lower. As shown in Table 2, TOC-729-1 and TOC-729-3 are both with a total uncertainty of 1.3×10^{-17} and the fractional uncertainty of the total systematic shift difference between the two TOCs is calculated as 1.9×10^{-17}.

4. Conclusion and perspectives

We reported an experimental demonstration of geopotential difference measurement using two transportable $^{40}Ca^{+}$ optical clocks in the laboratory with the same systematic uncertainty of 1.3×10^{-17}, which was limited by the uncertainty of BBR shift of each clock. The altitude differences were measured with total uncertainties at the level of 20 cm, which were in agreement with the results of geometrical measurement. After correcting the systematic shift (gravitational red shift included), the frequency difference of the two clocks was estimated to be -0.7×10^{-17} with a total uncertainty of 2.2×10^{-17}. It verified the reliability of the transportable $^{40}Ca^{+}$ optical clock at the low level of 10^{-17}. Considering the limitation of the instability of clock laser and the uncertainty of the BBR frequency shift, it was necessary to take some measures to further improve the clock precision. In the future, correlation spectroscopy can be employed to improve the instability of clock comparison by measuring the correlated atomic spectroscopy between the two clocks,[40] which provides a frequency difference measurement beyond the laser coherence time. For the clock systematic uncertainty, the BBR frequency shift of $^{40}Ca^{+}$ optical clock can be reduced further to 2.0×10^{-18} with an improved trap design and using a BBR shielding.[37] With these improvements, the transportable $^{40}Ca^{+}$ optical clocks will be developed towards an uncertainty at a low level of 10^{-18} at room temperature, fulfilling the requirement of establishing the global unified elevation network with a precision of centimeter and testing the validity of GR with high accuracy.

Acknowledgments

Project supported by the Basic Frontier Science Research Program of Chinese Academy of Sciences (Grant No. ZDBS-LY-DQC028), the National Key Research and Development Program of China (Grant No. 2017YFA0304404), and the National Natural Science Foundation of China (Grant No. 11674357).

References

[1] Brewer S M, Chen J S, Hankin A M, Clements E R, Chou C W, Wineland D J, Hume D B and Leibrandt D R 2019 *Phys. Rev. Lett.* **123** 033201
[2] Huntemann N, Sanner C, Lipphardt B, Tamm Chr and Peik E 2016 *Phys. Rev. Lett.* **116** 063001
[3] McGrew W F, Zhang X, Fasano R J, Schäffer S A, Beloy K, Nicolodi D, Brown R C, Hinkley N, Milani G, Schioppo M, Yoon T H and Ludlow A D 2018 *Nature* **564** 87
[4] Nicholson T L, Campbell S L, Hutson R B, Marti G E, Bloom B J, McNally R L, Zhang W, Barrett M D, Safronova M S, Strouse G F, Tew W L and Ye J 2015 *Nat. Commun.* **6** 6896
[5] Oelker E, Hutson R B, Kennedy C J, Sonderhouse L, Bothwell T, Goban A, Kedar D, Sanner C, Robinson J M, Marti G E, Matei D G, Legero T, Giunta M, Holzwarth R, Riehle F, Sterr U and Ye J 2019 *Nat. Photon.* **13** 714
[6] Riehle F, Gill P, Arias F and Robertsson L 2018 *Metrologia* **55** 188
[7] McGrew W F, Zhang X, Leopardi H, Fasano R J, Nicolodi D, Beloy K, Yao J, Sherman J A, Schäfer S A, Savory J, Brown R C, Römisch S, Oates C W, Parker T E, Fortier T M and Ludlow A D 2019 *Optica* **6** 448
[8] Lisdat C, Grosche G and Quintin N 2016 *Nat. Commun.* **7** 12443
[9] Chou C W, Hume D B, Rosenband T and Wineland D J 2010 *Science* **329** 1630
[10] Godun R M, Nisbet-Jones P B R, Jones J M, King S A, Johnson L A M, Margolis H S, Szymaniec K, Lea S N, Bongs K and Gill P 2014 *Phys. Rev. Lett.* **113** 210801
[11] Huntemann N, Lipphardt B, Tamm Chr, Gerginov V, Weyers S and Peik E 2014 *Phys. Rev. Lett.* **113** 210802
[12] Rosenband T, Hume D B, Schmidt P O, Chou C W, Brusch A, Lorini L, Oskay W H, Drullinger R E, Fortier T M, Stalnaker J E, Diddams S A, Swann W C, Newbury N R, Itano W M, Wineland D J and Bergquist J C 2008 *Science* **319** 1808

[13] Delva P, Lodewyck J, Bilicki S, Bookjans E, Rolland A, Baynes F N, Margolis H S and Gill P 2017 *Phys. Rev. Lett.* **118** 221102

[14] Arvanitaki A, Huang J and Van Tilburg K 2015 *Phys. Rev. D* **91** 015015

[15] Derevianko A and Pospelov M 2014 *Nat. Phys.* **10** 933

[16] Dix-Matthews B P, Schediwy S W, Gozzard D R, Savalle E, Esnault F X, Lévèque T, Gravestock C, D'Mello D, Karpathakis S, Tobar M and Wolf P 2021 *Nat. Commun.* **12** 515

[17] Kang H J, Yang J, Chun B J, Jang H, Kim B S, Kim Y J and Kim S W 2019 *Nat. Commun.* **10** 4438

[18] Shen Q, Guan J Y, Zeng T, Lu Q M, Huang L, Cao Y, Chen J P, Tao T Q, Wu J C, Hou L, Liao S K, Ren J G, Yin J, Jia J J, Jiang H F, Peng C Z, Zhang Q and Pan J W 2021 *Optica* **8** 471

[19] Takano T, Takamoto M, Ushijima I, Ohmae N, Akatsuka T, Yamaguchi A, Kuroishi Y, Munekane H, Miyahara B and Katori H 2016 *Nat. Photon.* **10** 662

[20] Bothwell T, Kennedy C J, Aeppli A, Kedar D, Robinson J M, Oelker E, Staron A and Ye J 2022 *Nature* **602** 420

[21] Mehlstäubler T E, Grosche G, Lisdat C, Schmidt P O and Denker H 2018 *Rep. Prog. Phys.* **81** 064401

[22] Grotti J, Koller S, Vogt S, *et al.* 2018 *Nat. Phys.* **14** 437

[23] Takamoto M, Ushijima I, Ohmae N, Yahagi T, Kokado K, Shinkai H and Katori H 2020 *Nat. Photon.* **14** 411

[24] Cao J, Zhang P, Shang J, Cui K, Yuan J, Chao S, Wang S, Shu H and Huang X 2017 *Appl. Phys. B* **123** 1

[25] Huang Y, Zhang H, Zhang B, Hao Y, Guan H, Zeng M, Chen Q, Lin Y, Wang Y, Cao S, Liang K, Fang F, Fang Z, Li T and Gao K 2020 *Phys. Rev. A* **102** 050802

[26] Stuhler J, Abdel Hafiz M, Arar B, Bawamia A, *et al.* 2021 *Meas. Sens.* **18** 100264

[27] Abbasov T, Makarenko K, Sherstov I, Axenov M, Zalivako I, Semerikov I, Borisenko A, Khabarova K, Kolachevsky N, Chepurov S, Taichenachev A, Bagaev S and Tausenev A 2020 arXiv: 2010.15244

[28] Cao J, Yuan J, Wang S, Zhang P, Yuan Y, Liu D, Cui K, Chao S, Shu H, Lin Y, Cao S, Wang Y, Fang Z, Fang F, Li T and Huang X 2022 *Appl. Phys. Lett.* **120** 054003

[29] Huang Y, Guan H, Zeng M, Tang L and Gao K 2019 *Phys. Rev. A* **99** 011401

[30] Shang J, Cao J, Cui K, Wang S, Zhang P, Yuan J, Chao S, Shu H and Huang X 2017 *Opt. Commun.* **382** 410

[31] Hendricks R J, Grant D M, Herskind P F, Dantan A and Drewsen M 2007 *Appl. Phys. B* **88** 507

[32] Ibaraki Y, Tanaka U and Urabe S 2011 *Appl. Phys. B* **105** 219

[33] Roos C F, Chwalla M, Kim K, Riebe M and Blatt R 2006 *Nature* **443** 316

[34] Huang P W, Tang B, Chen X, Zhong J Q, Xiong Z Y, Zhou L, Wang J and Zhan M S 2019 *Metrologia* **56** 045012

[35] Smarr L L, Vessot R F C, Lundquist C A, Decher R and Piran T 1983 *Gen. Relativ. Gravit.* **15** 129

[36] Ludlow A D, Boyd M M, Ye J, Peik E and Schmidt P O 2015 *Rev. Mod. Phys.* **87** 637

[37] Zhang P, Cao J, Yuan J, Liu D, Yuan Y, Wei Y, Shu H and Huang X 2021 *Metrologia* **58** 035001

[38] Dubé P, Madej A A, Bernard J E, Marmet L, Boulanger J S and Cundy S 2005 *Phys. Rev. Lett.* **95** 033001

[39] Yuan J B, Cao J, Cui K F, Liu D X, Yuan Y, Chao S J, Shu H L and Huang X R 2021 *Chin. Phys. B* **30** 070305

[40] Clements E R, Kim M E, Cui K, Hankin A M, Brewer S M, Valencia J, Chen J S, Chou C W, Leibrandt D R and Hume D B 2020 *Phys. Rev. Lett.* **125** 243602